

Université Laval

Département des Sciences Géomatiques

Laboratoire REPER 3D

From Data to Learning: A Comparative Study of UAV Photogrammetry Platforms for Educational Use in Urban Environments

Alexandre Laplante (alexandre.laplante.2@ulaval.ca)^a

Willian Ney Cassol (willian-ney.cassol@scg.ulaval.ca)^{a *}

Louis-Etienne Guimond (Louis-Etienne.Guimond@scg.ulaval.ca)^a

Vincent Dupont (vincent.dupont@scg.ulaval.ca)^a

^a Department of Geomatic sciences, Université Laval, 1055 Av. du Séminaire, Québec, QC G1V 0A6

*Correspondence: reper3d@scg.ulaval.ca

1 Abstract: This research investigates the quality of photogrammetric data acquired by low-
2 cost, mid-range, and high-performance drones in an urban context. A systematic, rigorous,
3 and repeatable methodology was developed to acquire, process, and analyze the data. The
4 study followed three phases: (1) planning and acquisition using various UAV platforms,
5 (2) processing the data according to standards, and (3) comparative analysis based on
6 sensor precision and geometric accuracy, using high-accuracy references. The results
7 highlight the strengths and limitations of each drone type in producing reliable urban
8 photogrammetric outputs. All data and products generated are openly accessible online and
9 intended for educational and institutional use, supporting teaching, training, and research
10 in geomatics and photogrammetry.

11 1. Introduction

12 Imaging aerial drones or unmanned aerial vehicles (UAVs) have increased the capacity of
13 acquiring geospatial data especially with their cost-effectiveness and flexibility when
14 compared to other acquisition systems (Ludwig et al. 2020). This photogrammetric data,
15 traditionally used for mapping, is now being applied in various other domains (Berteška
16 and Ruzgienė 2013). Rizo-Maestre et al. (2020) have proposed the incorporation of
17 photogrammetric techniques in architectural projects also considering BIM (Building
18 Information Modeling) instead of using classical work processes to avoid errors and reduce
19 time. In agriculture, Nebike et al. (2016) have investigated the performance of multispectral
20 sensors embedded in UAVs to predict grain yield and to detect plant diseases. Belmonte et
21 al. (2019) have considered UAV image-derived Structure-from-Motion (SfM) models and
22 high-resolution multi-spectral to quantify the structure of a forest in fine and mid-scales.

23 González-Jaramillo et al. (2019) and Bourgoïn et al. (2020) have also used UAVs to
24 estimate the biomass of tropical forest and to assess changes in forest structure. UAVs have
25 also been used in studying processes in the coastal areas (e.g. Scarelli et al. 2016; Pagan et
26 al. 2019) and for coastal management (e.g. Adade et al. 2021; Sim et al. 2018). The 3D
27 modeling for urban areas from photogrammetric approaches has a wide range of
28 applications (Barba et al. 2019a), from 3D archaeological modeling (Rinaudo et al. 2012)
29 to disaster monitoring (e.g. (Quaritsch et al. 2010; Rossi et al. 2018). Sohl et al. (2024)
30 have explored the potential of low-cost UAV in photogrammetric engineering. In this
31 research, the authors made an in-depth investigation of generating photogrammetric
32 models from a low-cost UAV, proposing an analysis of data quality.

33 A key factor when using UAVs is still the accuracy of geospatial data acquired and
34 consequently the quality of derived products (e.g. point clouds and orthoimages). This
35 quality is usually assessed considering Ground Control Points (GCP) and Check Points
36 (CP) (Martínez-Carricondo et al. 2018; Sanz-Ablanedo et al. 2018; Barba et al. 2019b).
37 Recently, ASPRS has adopted the Positional Accuracy Standards for Geospatial Data
38 (ASPRS 2024). "The publication of this new edition of the accuracy standards came in
39 response to evolving technologies and industry needs. It will have a positive and lasting
40 impact on geospatial capabilities and all who benefit from these ser-vices (...)" (ASPRS
41 2024). The main changes include the relaxation of the accuracy requirements for ground
42 control and checkpoints to accommodate a broader range of project conditions, thus
43 allowing for more practical and cost-effective implementations of geospatial data
44 collection. Furthermore, when computing the accuracy of a photogrammetric product, the
45 RMSE of checkpoints may be considered. Additionally, to improve the robustness of the

46 accuracy assessment process, the minimum number of checkpoints required for product
47 accuracy evaluation has been increased from 20 to 30. This change ensures that results are
48 based on a larger sample size, improving the representativeness and reliability of the
49 accuracy metrics. However, to maintain efficiency in large-scale projects, the maximum
50 number of checkpoints for accuracy assessment has been limited to 120, balancing the need
51 for detailed data with practical constraints. Finally, the introduction of the term three-
52 dimensional positional accuracy reflects a shift towards a more holistic approach to
53 geospatial accuracy, incorporating all spatial dimensions rather than focusing on radial and
54 vertical accuracy (adapted from ASPRS 2024). This manuscript is divided into three
55 sections. The first section describes the data acquisition systems, the data acquisition
56 methodology, and the processing of acquired data with generated products. The second
57 section presents the results and the discussion about the study area. The third section
58 concludes the paper with future perspectives and discusses the educational value of the
59 datasets and its potential use in teaching contexts.

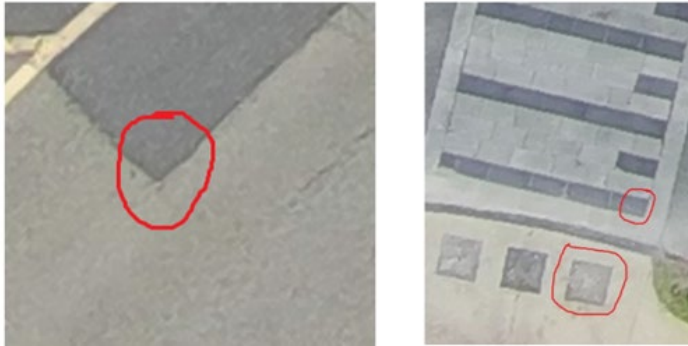
60 2. Materials and Methods

61 The acquisition of photogrammetric data does not only involve the acquisition of images
62 by the camera on board a drone platform. Indeed, to georeference the acquired images, it
63 is necessary to acquire control points. The check points are needed to control the quality of
64 point cloud and ortho mosaics generated. Hence, it is necessary to place targets on the
65 territory to be mapped (cf. the dimensions, distribution on the territory and required quality
66 in section F, annex III, ASPRS 2024). This section covers data acquisition, both in imagery
67 and in GNSS.

68 2.1. Data acquisition systems

69 A Trimble R12i GNSS receiver was used to acquire points in the field. This receiver has a
70 standard uncertainty estimated by the addition of the accuracy of the real-time corrections,
71 plus 5 mm and plus 0.4 mm per degree (Trimble 2020). The Trimble TSC5 handheld was
72 used. The pole used was a 2.00 m fixed carbon fiber pole. The surveys to acquire the control
73 points were carried out on 15-17, 20-22, 28 May and 25 June 2024. Three different drones
74 were used for this research namely: the EVO II Pro from Autel Robotics, the Mavic 3
75 Enterprise from DJI and the mdMapper 1000 DG from Micro-drones. The EVO II Pro is a
76 low-cost drone that can be purchased for around \$3000 CAD. It does not have a high-
77 precision GNSS antenna, the quality of its positioning in flight is around 1.5 m in
78 planimetry and 0.5 m in altimetry. It has a 20-megapixel Sony camera with a 1" CMOS
79 sensor (Autel Robotics 2022). The Mavic 3E is a mid-range drone that can be purchased
80 for around \$6,000 CAD. It is equipped with an RTK module that receives real-time
81 corrections to obtain an accuracy of 0.1 m. The real-time corrections were provided by the
82 Can-Net service. It has a 20-megapixel wide-angle camera with a 4/3" CMOS wide sensor
83 (DJI Enterprise 2024). The mdMapper 1000 DG is a high-end drone with an estimated cost
84 of around \$90,000 CAD considering the system's sensors. It is equipped with an APX15
85 navigation system, its flight positioning quality was on average 1.5 m, with a 42-megapixel
86 Sony RX1RII camera (Sony 2024). It is the only drone used that is considered high
87 performance due to the quality of the data acquired by these sensors.

101 Recommended control and check points include points that mark changes in color or
102 texture on the ground, such as new paving or pavers at grade. Examples of the points
103 surveyed on campus can be seen in Figure 2.



104

105 *Figure 2 - Type of GCP and CP in this project, the red circles show recommended points.*

106 To ensure systematic and rigorous photogrammetric analysis, the same flight parameters
107 were used during acquisitions for each of the drones. The acquisition parameters were a
108 flight height of 110m above the ground; a lateral overlap of 70%; a longitudinal overlap of
109 90 % and a speed of 4 m/s. All flights for the EVO II Pro and the Mavic 3E were carried
110 out in double grid for a better reconstruction of the territory to be mapped. A double grid
111 consists of making a flight pattern optimized according to the sector under study and a
112 second flight pattern where the flight lines are perpendicular to the first pattern. The flights
113 for the mdMapper 1000 DG were single grid because of its reduced autonomy compared
114 to other platforms. Note that carrying out surveys in single grid using the mdMapper 1000
115 DG drone produces high quality results compared to other drones used.

116 It is important to mention that for photogrammetric missions, the user must adapt the flight
117 parameters according to the project. The analysis of the parameters must be carried out
118 before each flight. For example, the flight speed directly impacts the quality of the acquired

133 *Table 1 - Characteristics of the flights over the Alphonse-Desjardins building.*

Drone	Flight time (minutes)	Number of images	Estimated GSD (cm)	Sizes of all images (GB)
mdMapper 1000 DG	17	191	1.42	3.02
Mavic 3E	18	376	2.96	3.85
EVO II pro	25	562	2.50	6.49

139 **2.3. Processing of acquired data**

140 To reduce the variables that could affect the final quality, the processing of the acquired
 141 data was carried out systematically with the same software for all the data from the different
 142 drones. The software used for the reconstruction of photogrammetric models and the
 143 generation of the photogrammetric products is UASMaster from Trimble Inpho (Trimble
 144 2024a). Before that, the PosPAC software from Trimble Applanix (Trimble 2024b) was
 145 used to correct the trajectory of the mdMapper 1000 DG in post-processing.

146 Georeferencing of the image blocks required the measurement of GCP. For each flight, an
 147 average of 15 GCP were chosen to have an optimal spatial distribution. The methodology
 148 used for measuring the points consisted of marking the pixel of each image where the
 149 physical element was clearly visible and easy to interpret. CP were used to validate the
 150 adjustment and georeferencing of the image blocks. To meet ASPRS standards (ASPRS
 151 2024, p.30), a minimum of 30 CP were selected in each image block. CP are of crucial
 152 importance in the validation of the generated photogrammetric products. Indeed, they make
 153 it possible to evaluate the differences between the data acquired by the photogrammetric

154 missions and the reference data on the study zone. In urban context, where the CP are
155 physical and permanent elements of the terrain, it is recommended to make a grid to
156 uniformly cover the entire sector under study (ASPRS 2024, p.31).

157 2.4. Generated products

158 For each acquired sector, a photogrammetric point cloud and a true orthoimage were
159 generated using UASMaster software. Figure 4 shows different renderings obtained with
160 the DJI Mavic 3E.



161

162 *Figure 4 - Extracts from the point cloud (left) and the orthoimage (right) of the Louis-Jacques Casault building and its*
163 *surroundings.*

164 All point clouds are publicly accessible via Université Laval's ArcGIS Online platform.
165 Hence, it is possible to navigate in a 3D Scene and explore the data using the QR codes
166 found in Figure 5 instead of just analyzing the figures in perspective.



167

168 *Figure 5 - QR code of the 3D Scenes containing the point clouds of each drone. A links to point cloud generated from*
169 *data acquired with mdMapper 1000DG, B with DJI Mavic E and C with Autel EVO II.*

170 Furthermore, an orthomosaic corresponding to each drone survey was produced. These
171 datasets are likewise publicly available through a web map hosted on Université Laval's
172 ArcGIS Online platform, accessible via the QR code shown in Figure 6. It should be
173 emphasized that the spatial resolution of the mosaics was intentionally reduced to 10 cm
174 to enhance online display performance and reduce storage usage on the ArcGIS Online
175 cloud platform. The point clouds, mosaics and orthoimages in their optimal spatial
176 resolution vary between 1.2 cm and 3.5 cm.



177

178 *Figure 6 - Drone ortho mosaics Campus UL Summer 2024*

179 3. Results and discussion

180 3.1. Processed data quality

181 ASPRS (2024) was considered to validate the photogrammetric processing and products
182 generated in this project. Although it is mainly based on aerial acquisitions by aircraft with

183 high-performance sensors, it is important to show the difference between this standard and
 184 the reality of sensors present on the market. According to ASPRS (2024), it states that the
 185 GCP and CP points must be 2 times more precise than the precision targeted for the final
 186 product (ASPRS 2024, p.18). Among the findings that will be presented in this section,
 187 special attention will be given to the CP. The latter better represents the quality that a
 188 professional could expect to obtain from a photogrammetric solution since they are
 189 independent of data processing.

190 The quality assessment of photogrammetric products is based on the Root Mean Square
 191 Error (RMSE), calculated by UASMaster during processing. To facilitate the interpretation
 192 of the results, a planimetric or radial RMSE (RMSE_r) and a vertical RMSE (RMSE_v) were
 193 calculated from the RMSE (x,y,z) for the check points and can be observed in the Appendix
 194 A. These results are summarized and presented in Tables 2, 3 and 4 showing the mean,
 195 maximum, minimum and standard deviation of the radial (horizontal or planimetry) and
 196 vertical (altimetry) differences for the sectors acquired during the summer of 2024 for each
 197 UAV used in this project. In Table 2, a standard deviation of 1.02 cm in planimetry and
 198 1.15 cm in altimetry demonstrates that the products generated using the mdMapper 1000
 199 DG remain consistent from one flight to another. A total of 18 missions were carried out.

200 *Table 2 - Summary of RMSE in planimetry and altimetry of the mdMapper 1000 DG*

	RMSE_r (cm)	RMSE_v (cm)
Mean	3.70	5.23
Maximum	6.40	7.49

Minimum	2.23	3.59
Standard deviation	1.02	1.15

201 In Table 3, a standard deviation of 0.29 cm in planimetry and 0.97 cm in altimetry can be
 202 observed. This demonstrates that the products generated using the Mavic 3E remain
 203 consistent from one flight to another, with a total of 17 missions performed. In addition,
 204 the mean RMSE in altimetry is less than 5 cm.

205 *Table 3 - Summary RMSE in planimetry and altimetry of the Mavic 3E*

	RMSE_r (cm)	RMSE_v (cm)
Mean	3.20	4.20
Maximum	3.84	6.97
Minimum	2.78	2.79
Standard deviation	0.29	0.97

206 In Table 4, a standard deviation of 0.66 cm in planimetry and 5.18 cm in altimetry was
 207 observed. The values concerning the altimetry deviations are significantly higher compared
 208 to other drones. These deviations demonstrate that the altimetry deviations are not always
 209 consistent from one flight to another with the EVO II Pro. A total of 17 missions were
 210 performed.

211 *Table 4 - Summary RMSE in planimetry and altimetry of the EVO II Pro*

	RMSE_r (cm)	RMSE_v (cm)
--	------------------------------	------------------------------

Mean	5.26	11.60
Maximum	6.92	23.97
Minimum	4.23	5.37
Standard deviation	0.66	5.18

212 From the data presented, it can be observed that the three acquisition platforms offer similar
 213 solutions. However, the mdMapper 1000 DG and the Mavic 3E have smaller RMSE than
 214 those obtained by the EVO II Pro, particularly in altimetry. Also, as proposed by ASPRS
 215 (2024), an uncertainty of 2 cm for CP and a GSD of 3 cm should allow for planimetry
 216 deviations of 4 cm. The deviations on the GCP and CP are the same magnitude for the
 217 mdMapper 1000DG and the Mavic 3E.

218 3.2. Data quality analysis

219 For the analysis of the highest deviations in planimetry and altimetry, two sectors may be
 220 investigated in detail. There is the entrance to the campus via Laurier Boulevard and the
 221 sector of the Community Gardens of Université Laval. The image blocks of the sector at
 222 the entrance to the campus via Laurier Boulevard present the greatest RMSE. However,
 223 the geospatial distribution of the GCP and CP in this sector is not optimal, probably
 224 affecting the final quality. Next, the Community Gardens sector was selected to analyze
 225 the highest deviations. The distribution of the GCP and CP is satisfactory in this sector,
 226 which allows us to conclude that this is not the only reason that it creates higher RMSE
 227 values. Other causes of higher RMSE, particularly in altimetry, would be abundant
 228 vegetation, as well as large surfaces with little texture, such as the sports fields and the

229 uniformly white roof of the Telus Stadium. Table 5 shows the RMSE of the GCP and CP
 230 for the three image blocks acquired in this sector. The RMSE obtained are similar for the
 231 mdMapper 1000 DG and the Mavic 3E, while the values of the EVO II Pro are higher,
 232 mainly in altimetry.

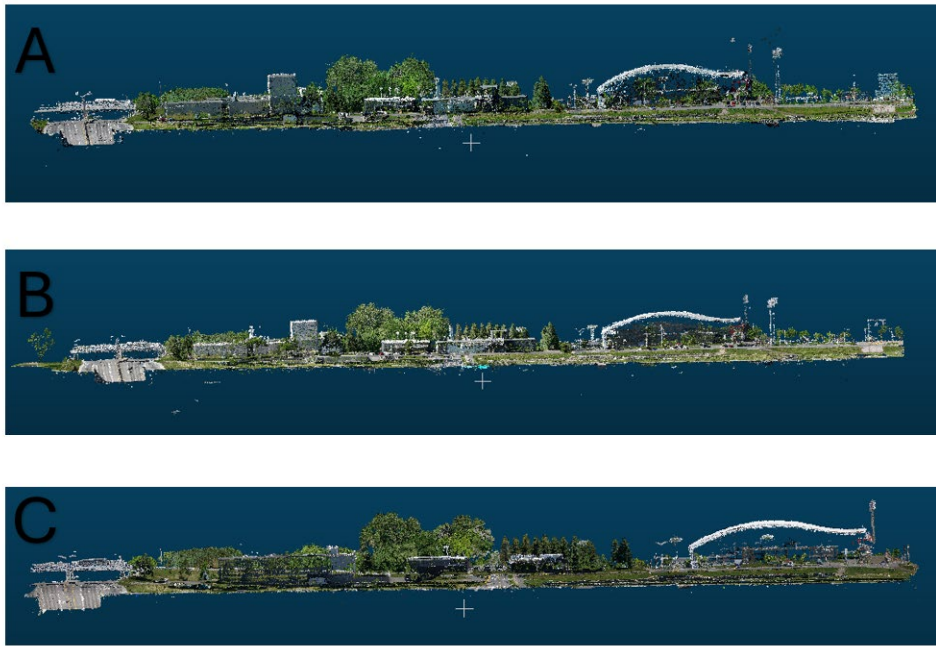
233 *Table 5 - Community Gardens sector.*

	GCP		CP	
	RMSEr (cm)	RMSEv (cm)	RMSEr(cm)	RMSEv (cm)
mdMapper 1000 DG	1.98	3.55	2.98	5.11
Mavic 3E	2.36	3.05	3.43	5.08
EVO II Pro	3.82	12.52	5.51	23.97

234

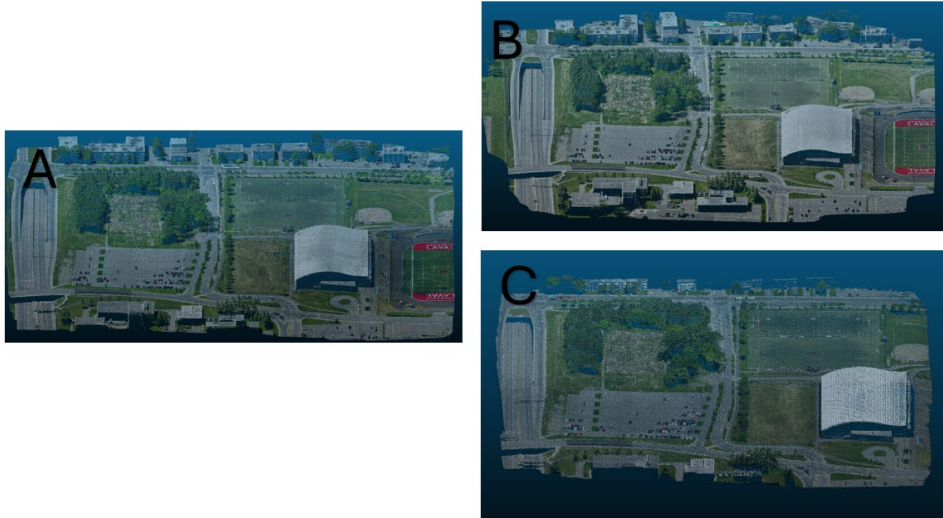
235 For the Community Gardens sector, it is also interesting to compare the point clouds
 236 generated by UASMaster. The biggest difference is the point density. It can be observed
 237 that the mdMapper 1000 DG point cloud has a considerably higher number of points than
 238 the Mavic 3E. For the latter, there are 9.5 million points, for the EVO II Pro there are 11.9
 239 million points and for the mdMapper 1000 DG there are 26.8 million points. In this sector,
 240 sparse noise was observed in the point clouds and this, for the three acquisitions carried
 241 out. However, it is observed that the mdMapper 1000 DG point cloud has slightly less noise
 242 than the other two-point clouds. This difference comes from the superior quality of the
 243 mdMapper 1000 DG camera, which is full-frame and calibrated. Figures 7 and 8 illustrate
 244 the different point clouds generated for the Université Laval Community Gardens area. A,

245 B and C illustrate, respectively, the point clouds generated from the images acquired by the
246 EVO II Pro, the Mavic 3E and the mdMapper 1000 DG. For a better visualization of the
247 point clouds, it is advisable to consult the full 3D scenes from the QR codes presented in
248 Figure 5.



249

250 *Figure 7 - Comparison of point clouds for the community garden sector; profile view. A was produced with data*
251 *acquired by EVO II Pro, B by the Mavic 3E and C by the mdMapper 1000 DG.*



252

253 *Figure 8 - Comparison of point clouds for the Community Gardens sector, perspective view. A was produced with data*
 254 *acquired by EVO II pro, B by the Mavic 3E and C by the mdMapper 1000 DG.*

255 For the analysis of the lowest planimetry and altimetry deviations, the Palasis-Prince and
 256 La Laurentienne buildings sector was chosen. Although it is not the sector with the lowest
 257 deviations, it is the sector with the most interesting results for the three drones (cf. Table
 258 6). By observing the CP, the planimetric and altimetric deviations are all less than 5.5 cm.
 259 These satisfactory deviations are probably due to the topography of the terrain, which is
 260 relatively flat, the physical elements on the terrain which allow to obtain more points during
 261 the 3D reconstruction and the flight conditions which were conducive to acquisition. Thus,
 262 there was little wind, and the cloud cover prevented the formation of shadows on the
 263 ground. The reconstruction of these models allowed low RMSE.

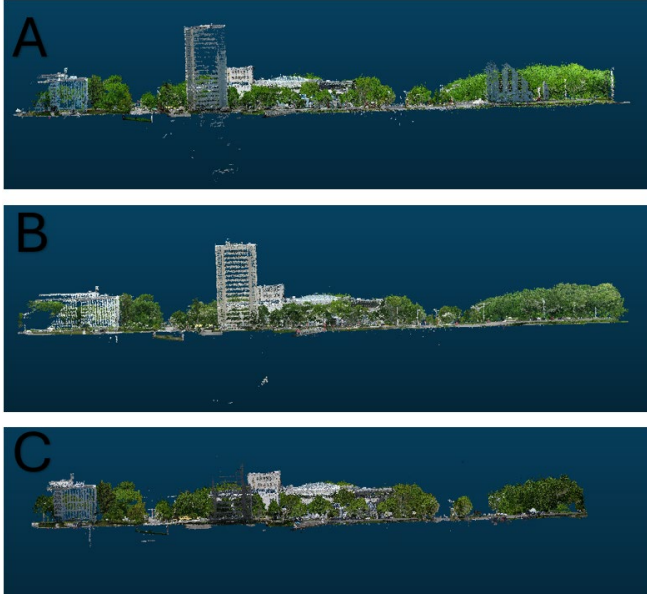
264 *Table 6 - Palasis-Prince and La Laurentienne sector.*

GCP		CP	
RMSEr (cm)	RMSEv (cm)	RMSEr (cm)	RMSEv (cm)

mdMapper 1000 DG	2.22	2.41	2.48	5.01
Mavic 3E	2.15	1.31	3.11	5.36
EVO II Pro	2.60	1.75	4.80	5.37

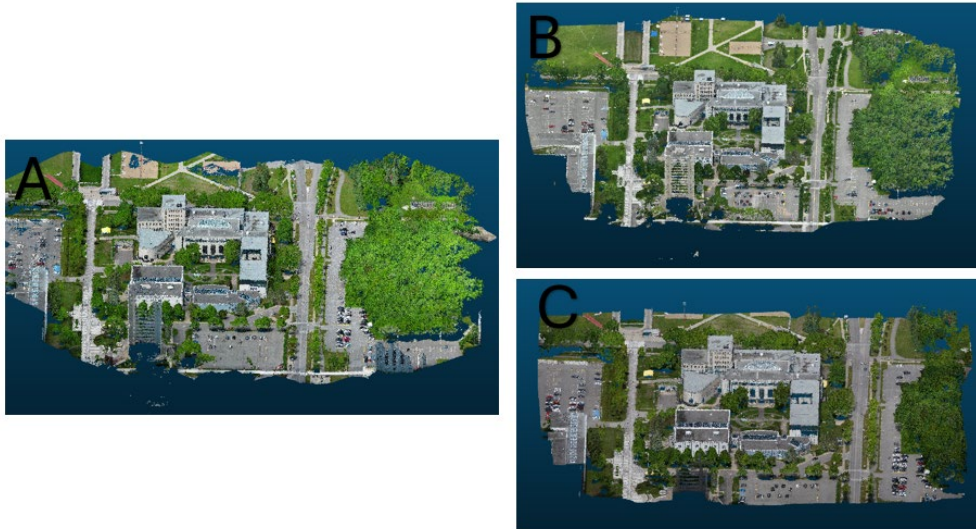
265

266 For the Palasis-Prince and La Laurentienne buildings sector, it is also interesting to
 267 compare the generated point clouds. The first observation is that the point clouds, generated
 268 from the acquisitions by the different drones, all have a similar number of points. For the
 269 Mavic 3E there are 6.8 million points, for the EVO II Pro there are 7.7 million points, for
 270 the mdMapper 1000 DG there are 6.8 million points. Despite this, there is a significant
 271 difference between the rendering of the mdMapper 1000 DG and the renderings of the
 272 Mavic 3E and the EVO II Pro. The main difference is that there are more points on the
 273 facades of the buildings in the clouds generated by the Mavic 3E and the EVO II pro. Such
 274 difference comes from the dual grid parameter used for these drones. Another advantage
 275 of the dual grid is that it increases the number of images, allowing better coverage on
 276 building facades and facilitating the 3D reconstruction of these surfaces. However, there is
 277 a big difference in the noise of the point cloud generated from the mdMapper 1000 DG.
 278 Indeed, the rendering of the mdMapper 1000 DG is of better quality than the other two
 279 drones. Figures 9 and 10 allow a comparison between the point clouds generated for the
 280 Palasis-Prince and La Laurentienne buildings area of Université Laval. A, B and C
 281 illustrate, respectively, the point clouds generated from the images acquired by the EVO II
 282 Pro, the Mavic 3E and the mdMapper 1000 DG.



283

284 *Figure 9 - Comparison of point clouds for the Palasis-Prince and La Laurentienne sectors, profile view. A was*
 285 *produced with data acquired by EVO II Pro, B by the Mavic 3E and C by the mdMapper 1000 DG.*



286

287 *Figure 10 - Comparison of point clouds for the Palasis-Prince and La Laurentienne sectors, perspective view. A was*
 288 *produced with data acquired by EVO II Pro, B by the Mavic 3E and C by the mdMapper 1000 DG.*

289 **3.3. Discussion**

290 Analyzing the processing reports generated by UASMaster, the image resolution for the
291 Louis-Jacques Casault sector varies across platforms: 2.65 cm for the EVO II Pro, 3.27 cm
292 for the Mavic 3E, and 1.52 cm for the mdMapper 1000 DG. These differences are primarily
293 due to the varying characteristics of the drones' cameras. Notably, while both the EVO II
294 Pro and the Mavic 3E are equipped with 20-megapixel sensors and flew at the same altitude
295 of 110 meters, their optical systems differ slightly, resulting in distinct GSD. This variation
296 in image resolution provides an interesting basis for comparing the RMSEr relative to
297 GSD. As shown in Table 10, the block of images acquired with the mdMapper 1000 DG
298 yielded a planimetric RMSEr of 3.87 cm approximately 2.55 times the image pixel size. In
299 contrast, the EVO II Pro resulted in a higher RMSEr of 5.35 cm, but a smaller relative ratio
300 of 2.02 times its GSD. According to ASPRS (2024), best practices recommend a GSD
301 approximately half the desired positional accuracy. In that context, the results from the
302 mdMapper 1000 DG and the EVO II Pro appear consistent and within expected tolerances.

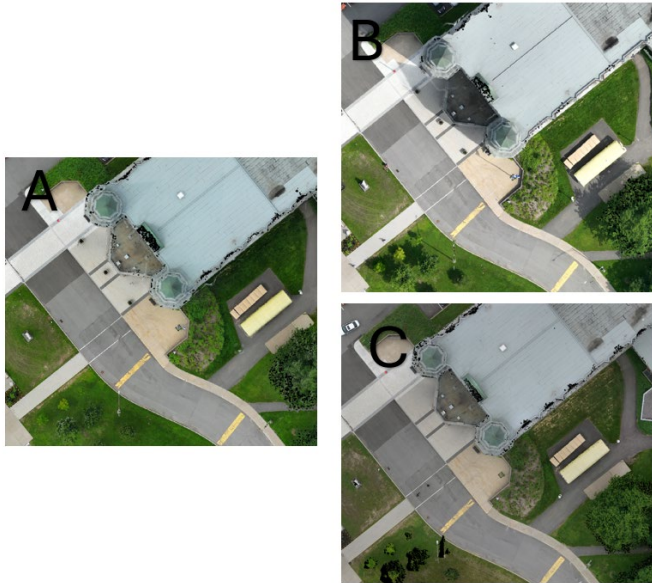
303 *Table 7 - Presentation of the RMSEr/GSD ratio.*

	GSD (cm)	RMSEr (CP) (cm)	Ratio (RMSEr /GSD)
mdMapper 1000 DG	1.52	3.87	2.55
Mavic 3E	3.27	2.78	0.85
EVO II pro	2.65	5.35	2.02

304

305 Interestingly, the Mavic 3E produced a planimetric RMSEr of only 2.78 cm less than its
306 GSD of 3.27 cm, yielding a ratio of 0.85. This surprisingly high level of accuracy may
307 result from several contributing factors. The Mavic 3E is equipped with a wide-angle lens,
308 which increases pixel size but also enhances scene coverage. Moreover, this drone offers
309 the highest positioning accuracy during data acquisition among the three, improving
310 georeferencing during photogrammetric processing. The dual-grid flight pattern used in the
311 Mavic 3E mission likely contributed as well, increasing the number of images where
312 control and check points are measured, thus enhancing overall spatial accuracy. To further
313 illustrate the output quality, Figure 11 presents an extract of the true orthoimages generated
314 from each drone. Visual inspection reveals noticeable shadows in the Mavic 3E results (see
315 Figure 9B), whereas the orthoimages from the EVO II Pro and the mdMapper 1000 DG
316 (Figures 9A and 9C, respectively) appear free of such artifacts. Variability in shadow
317 presence across the mosaics also observable via the ArcGIS Online viewer is influenced
318 by scene illumination conditions at the time of flight. Shadow orientation and length vary
319 depending on sun elevation, which affects the homogeneity of the final product. To achieve

320 more uniform renderings and reduce shadow interference, image acquisition under
321 consistent cloud cover is ideal, as it minimizes brightness variation across the scene.



322

323 *Figure 11 - Extracts of the orthoimages for the Louis-Jacques Casault sector. A was produced by the EVO II Pro, B by*
324 *the Mavic 3E and C by the mdMapper 1000 DG.*

325 4. Conclusion

326 This study provides a comprehensive evaluation of the photogrammetric performance of
327 three UAV platforms in urban environments, offering valuable insights into their respective
328 strengths and limitations. Notably, the DJI Mavic 3E demonstrates precision on par with
329 the high-end mdMapper 1000 DG, particularly in terms of the RMSEr/resolution ratio,
330 while the EVO II Pro performs admirably within its price range, confirming its suitability
331 for budget-conscious applications. Although the Mavic 3E and EVO II Pro exhibit greater
332 noise levels compared to the mdMapper 1000 DG, this can be effectively mitigated through

333 post-processing, and their use of a double-grid flight pattern contributes to enhanced visual
334 detail in final outputs.

335 Beyond technical analysis, a core objective of this initiative was to foster learning through
336 the creation of high-quality, openly accessible photogrammetric datasets. These resources
337 serve as a powerful foundation for hands-on education in geomatics, photogrammetry, and
338 urban mapping, particularly in contexts with limited access to UAV technology or
339 commercial data. The standardized methodology and open availability of these datasets not
340 only promote reproducibility and technical skill development but also illustrate the
341 principles of open science and collaborative learning. By enabling users to replicate
342 workflows, evaluate accuracy, and explore advanced applications such as machine learning
343 and change detection, the project has the potential to support a wide range of
344 interdisciplinary academic activities.

345 Future research could expand this comparative framework by incorporating additional
346 UAV models, diverse sensor types, as multispectral, hyperspectral, and LiDAR, and by
347 testing platform performance across varied environmental and geographic settings.
348 Furthermore, exploring temporal metrics and the integration of artificial intelligence for
349 automated monitoring would significantly enrich our understanding of UAV capabilities.
350 Ultimately, this work underscores the dual value of UAV-based photogrammetry as both a
351 technical tool and an educational asset in the geospatial sciences.

352 **Data Availability Statement:** All data considered in this manuscript can be viewed on
353 ArcGIS Online through QR codes inserted in the paper. Data is also available by the FRDR:
354 <https://www.frdr-dfdr.ca/repo/dataset/86ba16e7-7804-418d-913e-43978fa07f95>.

355 **Conflicts of Interest:** The authors declare no conflicts of interest. Please note that the
 356 authors of this article and the Université Laval staff members involved in this research
 357 compared the platforms presented in this article without any prior assumptions about their
 358 performance. In other words, this article does not make any recommendations for the use
 359 of a particular platform in private practice. Each platform was used and objectively
 360 evaluated with the same criteria and methods to show the quality of the photogrammetric
 361 data and the products generated from drone imagery in an urban context.

362 Appendix A

363 Tables A1, A2 and A3 present the RMSEr and RMSEv obtained for the GCP and CP,
 364 respectively for the mdMapper 1000 DG, Mavic 3E and EVO II Pro drones.

365 *Table A1 - Presentation of RMSEr and RMSEv of mdMapper 1000 DG data (see Appendix B for sector code).*

mdMapper 1000 DG				
	GCP		CP	
Sector	RMSEr (cm)	RMSEv (cm)	RMSEr (cm)	RMSEv (cm)
DKN&BON	2.03	2.99	3.57	4.38
PAL&LAU	2.22	2.41	2.48	5.01
Stadium	2.99	3.36	4.39	7.49
ABP&MDE	2.91	1.90	4.56	6.45
VND	2.23	2.70	2.72	5.54

LCT&CMT	2.63	2.63	3.93	3.59
ADJ	3.85	2.55	4.15	6.17
PRN	2.92	2.06	4.37	4.65
Volumetry	1.82	3.15	2.23	3.88
Garden	1.98	3.55	2.89	5.11
PEPS ¹	----			
Tours	2.99	2.89	2.94	4.47
PLT ²	3.38	2.22	4.86	6.47
VCH	2.44	3.05	2.95	3.67
GBI	3.16	1.88	3.74	4.66
CSL	2.37	1.78	3.87	4.29
Laurier Entrance	5.49	2.39	6.40	6.77
Parking 222	1.97	3.01	2.80	6.32

366 *1 Data not acquired.*

367 *2 Data acquired in the summer of 2023.*

368

369 *Table A2 - Presentation of RMSEr and RMSEV of Mavic 3E data (see Appendix B for sector code).*

Mavic 3E

GCP

CP

Sector	RMSEr (cm)	RMSEv (cm)	RMSEr (cm)	RMSEv (cm)
DKN&BON	1.84	1.62	3.19	3.74
PAL&LAU	2.15	1.31	3.11	5.36
Stadium	2.38	2.79	3.02	6.97
ABP&MDE	1.72	1.71	3.28	2.79
VND	2.92	1.83	3.57	3.65
LCT&CMT	3.06	2.37	3.52	3.79
ADJ	1.83	3.02	3.14	3.80
PRN	2.08	1.63	2.87	4.80
Parking 222	1.27	2.12	2.96	3.91
Garden	2.36	3.05	3.43	5.08
PEPS	1.20	1.80	2.89	3.29
Tours	2.10	2.04	2.97	3.31
PLT	2.92	1.99	3.84	4.69
VCH	2.10	2.08	3.12	4.15
GBI	1.97	1.33	3.09	4.32
CSL	1.46	2.96	2.78	3.25
Laurier Entrance	3.17	2.58	3.65	4.44

371 *Table A3 - Presentation of RMSEr and RMSEV of EVO II Pro data (see Appendix B for sector code).*

EVO II Pro				
	GCP		CP	
Sector	RMSEr (cm)	RMSEv (cm)	RMSEr (cm)	RMSEv (cm)
DKN&BON	3.92	3.66	5.47	12.24
PAL&LAU	2.60	1.75	4.80	5.37
Stadium	4.27	6.15	5.10	13.24
ABP&MDE	3.10	9.04	4.23	11.96
VND	4.80	8.72	4.46	10.65
LCT&CMT	3.52	0.13	4.59	6.19
ADJ	2.55	2.36	4.81	6.83
PRN	4.15	2.59	5.96	7.05
Parking 222	3.80	4.47	5.31	8.39
Garden	3.82	12.52	5.51	23.97
PEPS	4.43	6.90	5.17	18.08
Tours	3.72	5.30	5.44	18.59
PLT	3.88	3.76	5.88	10.12

VCH	3.06	3.99	5.97	8.22
GBI	1.69	0.71	4.50	7.46
CSL	3.45	5.71	5.35	10.00
Laurier Entrance	5.13	5.30	6.92	18.90

372 Appendix B

373 This section presents the codes allowing a better understanding of Tables 2, 3 and 4 with
 374 the name of different sectors of Université Laval Campus in Quebec City.

375 *Table B1 - Sector codes.*

DKN&BON	Charles-De Koninck & Jean-Charles- Bonenfant
PAL&LAU	Palasis-Prince and La Laurentienne
Stadium	Telus stadium and football field
ABP&MDE	Abitibi-Price & Dentistry
VND	Ferdinand- Vandry & Héma -Quebec
LCT&CMT	Agathe -Lacerte & Paul Comtois
ADJ	Alphonse-Desjardins
PRN	Alphonse-Marie-Parents

	Parking 222 to the South-East of Louis-Jacques-
Parking 222	Casault
Garden	Community garden
PEPS	PEPS
Tours	Felix-Antoine-Savard & Jeanne-Lapointe
PLT	Adrien-Pouliot
VCH	Alexandre Vachon
GBI	Gerard- Bisailon
CSL	Louis-Jacques- Casault
Laurier Entrance	Entrance to the campus via Laurier Boulevard

376

377 **Acknowledgments:** We would like to thank Université Laval for giving us access to the
378 equipment and installations to carry out this project. We also thank the Faculty of Forestry,
379 Geography and Geomatics, NSERC and FRQNT for their financial support. We would also
380 like to warmly acknowledge the involvement of Guy Montreuil in the acquisition of drone
381 data in the field. We extend a big thank you to Jonathan Gagnon, Cliford Vilpique, Marie-
382 Claude Boulet and Élisabeth Dionne for their involvement during the acquisition missions.

383 References

- 384 Ludwig, M.; M. Runge, C.; Friess, N.; Koch, T.L.; Richter, S.; Seyfried, S.; Wraase, L.;
- 385 Lobo, A.; Sebastià, M.-T.; Reudenbach, C.; et al. Quality Assessment of Photogrammetric
- 386 Methods—A Workflow for Reproducible UAS Orthomosaics. *Remote Sens.* 2020, 12,
- 387 3831. <https://doi.org/10.3390/rs12223831>
- 388 Berteška, T.; Ruzgienė, B. Photogrammetric mapping based on UAV imagery. *Geodesy*
- 389 *and Cartography.* 2013, vol. 39 issue 4, Pp. 158-163.
- 390 <https://doi.org/10.3846/20296991.2013.859781>
- 391 Rizo-Maestre, C.; González-Avilés, Á.; Galiano-Garrigós, A.; Andújar-Montoya, M.D.;
- 392 Puchol-García, J.A. UAV + BIM: In-corporation of Photogrammetric Techniques in
- 393 Architectural Projects with Building Information Modeling Versus Classical Work
- 394 Processes. *Remote Sens.* 2020, 12, 2329. <https://doi.org/10.3390/rs12142329>
- 395 Nebiker, S.; Lack, N.; Abächerli, M.; Läderach, S. Light-weight Multispectral UAV
- 396 Sensors and their capabilities for predicting grain yield and detecting plant diseases.
- 397 *ISPRS-Int. Arch. Photogramm. Remote Sens. Spat. Inf. Sci.* 2016, 41, 963–970.
- 398 Belmonte, A.; Sankey, T.; Biederman, J.A.; Bradford, J.; Goetz, S.J.; Kolb, T.; Woolley,
- 399 T. UAV-derived estimates of forest structure to inform ponderosa pine forest restoration.
- 400 *Remote Sens. Ecol. Conserv.* 2019.
- 401 González-Jaramillo, V.; Fries, A.; Bendix, J. AGB Estimation in a Tropical Mountain
- 402 Forest (TMF) by Means of RGB and Mul-tispectral Images Using an Unmanned Aerial
- 403 Vehicle (UAV). *Remote Sens.* 2019, 11, 1413.

404 Bourgoin, C.; Betbeder, J.; Couteron, P.; Blanc, L.; Dessard, H.; Oszwald, J.; Roux, R.L.;
405 Cornu, G.; Reymondin, L.; Mazzei, L.; et al. UAV-based canopy textures assess changes
406 in forest structure from long-term degradation. *Ecol. Indic.* 2020, 115, 106386.

407 Scarelli, F. M.; Cantelli, L.; Barboza, E. G.; Rosa, M. L. C. C.; Gabbianelli, G. Natural
408 and anthropogenic coastal system comparison using DSL from a low-cost UAV survey
409 (Capao Novo, RS/Brazil). *Journal of Coastal Research*, 2016, 75, Pp. 1232-1236.

410 Pagan, J.I.; Banon, L.; Lopez, I.; Banon, C.; Aragones, L. Monitoring the dune-beach
411 system of Guardamar del Segura (Spain) using UAV, SfM and GIS techniques. *Science of*
412 *the total environment*, 2019, 687, Pp. 1034-1045.

413 Adade, R.; Aibinu, A. M.; Ekumah, B.; Asaana, J. Unmanned Aerial Vehicle (UAV)
414 applications in coastal zone management – a review. *Environ Monit Assess*,
415 2021, 193:154.

416 Sim, S.; Song, D. Evaluation of cadastral discrepancy and continuous cadastral mapping
417 in coastal zone using unmanned aerial vehicle. *Journal of Coastal Research*, 2018, 85, Pp.
418 1386-1390.

419 Barba, S.; Barbarella, M.; Di Benedetto, A.; Fiani, M.; Gujski, L.; Limongiello, M.
420 Accuracy Assessment of 3D Photogrammetric Models from an Unmanned Aerial Vehicle.
421 *Drones* 2019a, 3, 79. <https://doi.org/10.3390/drones3040079>

422 Rinaudo, F.; Chiabrandò, F.; Lingua, A.; Spanò, A. Archaeological site monitoring: UAV
423 photogrammetry can be an answer. *Int. Arch. Photogramm. Remote Sens. Spat. Inf. Sci.*
424 2012, XXXIX-B5, 583–588.

425 Quaritsch, M.; Kruggl, K.; Wischounig-Strucl, D.; Bhattacharya, S.; Shah, M.; Rinner, B.
426 Networked UAVs as aerial sensor network for disaster management applications. *e & i*
427 *Elektrotechnik Und Inf.* 2010, 127, 56–63.

428 Rossi, G., Tanteri, L., Tofani, V. et al.; Multitemporal UAV surveys for landslide mapping
429 and characterization. *Landslides* 15, 1045–1052 (2018). [https://doi.org/10.1007/s10346-](https://doi.org/10.1007/s10346-018-0978-0)
430 018-0978-0

431 Sohl, M.A.; Mahmood, S.A. Low-cost UAV in photogrammetric engineering and remote
432 sensing: georeferencing, DEM accuracy, and geospatial analysis. *Journal of*
433 *Geovisualization and Spatial Analysis*, 8:14, 2024. 10.1007/s41651-024-00176-2

434 Martínez-Carricondo, P.; Agüera-Vega, F.; Carvajal-Ramírez, F.; Mesas-Carrascosa, F.-J.;
435 García-Ferrer, A.; Pérez-Porras, F.-J. Assessment of UAV-photogrammetric mapping
436 accuracy based on variation of ground control points. *Int. J. Appl. Earth Obs. Geoinf.*
437 2018, 72, 1–10.

438 Sanz-Ablanedo, E.; Chandler, J.H.; Rodríguez-Pérez, J.R.; Ordóñez, C. Accuracy of
439 Unmanned Aerial Vehicle (UAV) and SfM Photogrammetry Survey as a Function of the
440 Number and Location of Ground Control Points Used. *Remote Sens.* 2018, 10, 1606.

441 Barba, S.; Barbarella, M.; Di Benedetto, A.; Fiani, M.; Limongiello, M. Quality
442 assessment of UAV photogrammetric archaeological survey. *Int. Arch. Photogramm.*
443 *Remote Sens. Spat. Inf. Sci.* 2019b, XLII-2/W9, 93–100.

444 ASPRS. ASPRS Positional Accuracy Standards for Digital Geospatial Data. 2024 Edition
445 2, Version 2. 228 pages. Available at: <https://www.asprs.org/homefeatured/asprs->

446 approves-edition-2-version-2-of-the-asprs-positional-accuracy-standards-for-digital-
447 geospatial-data-2024.html . Accessed December 16th, 2024.

448 Trimble. Trimble R12i GNSS System. 2020. Datasheet available at
449 [https://trl.trimble.com/docushare/dsweb/Get/Document-951406/022516-511E-en-](https://trl.trimble.com/docushare/dsweb/Get/Document-951406/022516-511E-en-US_TrimbleR12i_SpecSheet_A4_0424_LR%20-%20sec.pdf)
450 [US_TrimbleR12i_SpecSheet_A4_0424_LR%20-%20sec.pdf](https://trl.trimble.com/docushare/dsweb/Get/Document-951406/022516-511E-en-US_TrimbleR12i_SpecSheet_A4_0424_LR%20-%20sec.pdf) . Accessed December 16th,
451 2024.

452 Autel Robotics. EVO II Pro Specifications. 2024.
453 <https://shop.autelrobotics.com/pages/evo-ii-pro-specification> . Accessed De-cember 16th,
454 2024.

455 DJI Enterprise. DJI Mavic 3 Enterprise Specs. 2024. [https://enterprise.dji.com/mavic-3-](https://enterprise.dji.com/mavic-3-enterprise/specs)
456 [enterprise/specs](https://enterprise.dji.com/mavic-3-enterprise/specs) . Accessed December 16th, 2024.

457 Sony. Sony RX1 RII Specifications & Features. 2024.
458 [https://www.sony.com/za/electronics/cyber-shot-compact-cameras/dsc-](https://www.sony.com/za/electronics/cyber-shot-compact-cameras/dsc-rx1rm2#product_details_default)
459 [rx1rm2#product_details_default](https://www.sony.com/za/electronics/cyber-shot-compact-cameras/dsc-rx1rm2#product_details_default). Accessed December 16th, 2024.

460 Trimble. Trimble Inpho UASMaster. 2024a.
461 <https://geospatial.trimble.com/en/products/software/trimble-inpho-uasmaster> . Accessed
462 December 16th, 2024.

463 Trimble Applanix. POSPac UAV. 2024b. [https://www.applanix.com/products/pospac-](https://www.applanix.com/products/pospac-uav.htm)
464 [uav.htm](https://www.applanix.com/products/pospac-uav.htm) . Accessed December 16th, 2024.